Supporting Information

1 CC2-based force field parameters

Table 1: CC2-based force field parameters (in a.u.) of methanol

Typ	x	y	z
Coordinates of O	-2.021250000	-0.386646667	0.000000000
Coordinates of H_1	-2.039730000	-2.193986667	0.000000000
Coordinates of C	0.509340000	0.443083333	0.000000000
Coordinates of H_2	0.469760000	2.500623333	0.000000000
Coordinates of H_3	1.540940000	-0.181536667	1.682290000
Coordinates of H_4	1.540940000	-0.181536667	-1.682290000
Dipole Moment	0.523133	-0.383806	0.000000
Quadrupole tensor (traceless)	-2.365014	1.686969	0.000000
	1.686969	2.959141	0.000000
	0.000000	0.000000	-0.594126
Polarizability tensor	22.846113	1.311812	0.000000
	1.311812	21.164068	0.000000
	0.000000	0.000000	20.183847

Table 2: CC2-based force field parameters (in a.u.) of 2-propanol

Typ	x	y	z
Coordinates of C_1	0.497550833	-2.486309167	0.612220000
Coordinates of H_1	0.519800833	-2.574899167	2.670950000
Coordinates of H_2	2.444010833	-2.524309167	-0.069340000
Coordinates of H_3	-0.472179167	-4.154539167	-0.107500000
Coordinates of C_2	-0.807779167	-0.108529167	-0.280490000
Coordinates of H_4	-2.759479167	-0.115299167	0.431400000
Coordinates of C_3	0.505260833	2.264390833	0.646520000
Coordinates of O	-0.844389167	-0.215069167	-2.961330000
Coordinates of H_5	-1.602599167	1.304070833	-3.588040000
Coordinates of H_6	-0.450539167	3.960980833	-0.041270000
Coordinates of H_7	0.513630833	2.343940833	2.707510000
Coordinates of H_8	2.456710833	2.305570833	-0.020630000
Dipole Moment	-0.19308	0.457852	0.395296
Quadrupole tensor (traceless)	0.679470	-1.431169	0.916482
	-1.431169	0.824159	-3.118022
	0.916482	-3.118022	-1.503630
Polarizability tensor	42.648902	-0.217346	1.491531
	-0.217346	48.428723	-0.479019
	1.491531	-0.479019	45.991990

Table 3: CC2-based force field parameters (in a.u.) of tetrachloromethane

Typ	x	y	z
Coordinates of C	0.000000000	0.000000000	0.000000000
Coordinates of Cl_1	2.718816816	0.000000000	1.922493807
Coordinates of Cl_2	-2.718816816	0.000000000	1.922493807
Coordinates of Cl_3	0.000000000	2.718816816	-1.922493807
Coordinates of Cl_4	0.000000000	-2.718816816	-1.922493807
Isotropic polarizability		70.0152211123	

2 CCS-based energies, transition frequencies and shifts

To investigate the influence of electron correlation on the solvent shifts of the emission energies and transition frequencies, we performed 2c-PERI-CCS (coupled cluster singles) calculations which utilized the same computational setup, i.e. basis sets, structures and embedding potentials, as the 2c-PERI-CC2 computations.
In the main paper, the influence of the environment on the phosphorescence energies and lifetimes of the state $^3A_2$ was investigated. While this state was obtained to be the energetically lowest excited state from all 161 2c-CC2 and 2c-PERI-CC2 calculations, the ordering of the states is changed if electron correlation effects are neglected. For the vacuum case, the ordering obtained from a 1c-CCS computation is $^3A_1$, $^3A_2$ and $^1A_2$ with increasing energy. The same ordering is obtained in 158 of the 161 2c-CCS and 2c-PERI-CCS computations. In three cases, however, a singlet state was energetically lower than the triplet state of interest.

2.1 Phosphorescence energies and their shifts

The phosphorescence energies based on the 2c-CCS and 2c-PERI-CCS methods are given in Table 4. The resulting solvent shifts are visualized in Figure 1 which can be compared to Figure 1 in the main paper. Qualitatively, both methods give rise to the same trends. However, the shifts differ significantly in magnitude.

Table 4: Vertical 2c-sPERI-CCS and 2c-CCS emission energies (ΔE in eV) of the state $^3A_2$ of 4*H*-pyran-4-thione in different environments.

	$k0p0$	$k0p1$	$k2p2$
2-PrOH	2.92 ± 0.00	3.24 ± 0.09	3.54 ± 0.39
MeOH	2.90 ± 0.00	3.12 ± 0.04	3.00 ± 0.29
CCl_4	2.68 ± 0.00	3.03 ± 0.11	3.03 ± 0.11
vacuum	2.74	2.74	2.74

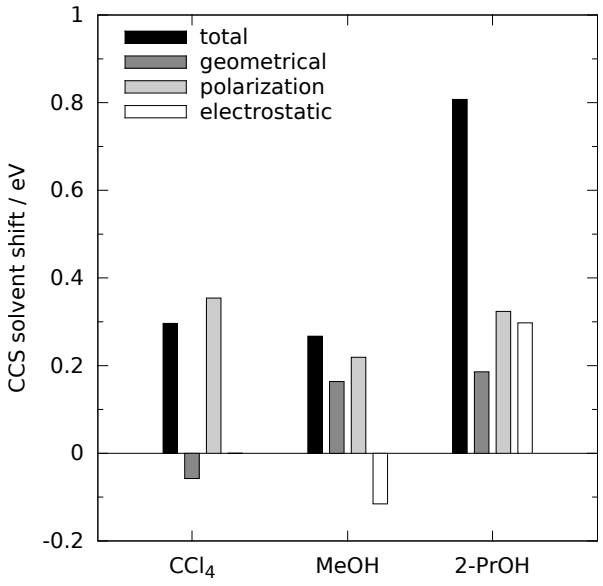

Figure 1: Solvent shifts of averaged phosphorescence energies obtained from 2c-PERI-CCS computations

2.2 Phosphorescence transition frequencies and their shifts

It was assumed that phosphorescence takes place only if no singlet state is lower in energy than the triplet state of interest. Otherwise, fluorescence is expected. Therefore, phosphorescence frequencies obtained from 2c-PERI-CCS computations which yielded a lower lying singlet state were neglected.

The averaged phosphorescence frequencies based on the 2c-CCS and 2c-PERI-CCS methods are given in Table 4 and visualized in Figure 2. Qualitatively, both the CC2 and CCS based methods give rise to similar trends. However, both the absolute frequencies and the relative shifts differ significantly.

Table 5: Total phosphorescence frequencies in $(\mathrm{ms})^{-1}$ of $^3\mathrm{A}_2$ of 4*H*-pyran-4-thione obtained from N single-point calculations for different environments.

	$k0p0$	N	$k0p1$	N	$k2p2$	N
2-PrOH	15.1 ± 0.0	20	32.1 ± 5.8	20	32.8 ± 13.6	19
MeOH	15.1 ± 0.0	20	26.3 ± 2.5	20	23.5 ± 7.7	18
CCl_4	15.5 ± 0.0	20	31.2 ± 8.5	20	31.2 ± 8.5	20
vacuum	15.8	1	15.8	1	15.8	1

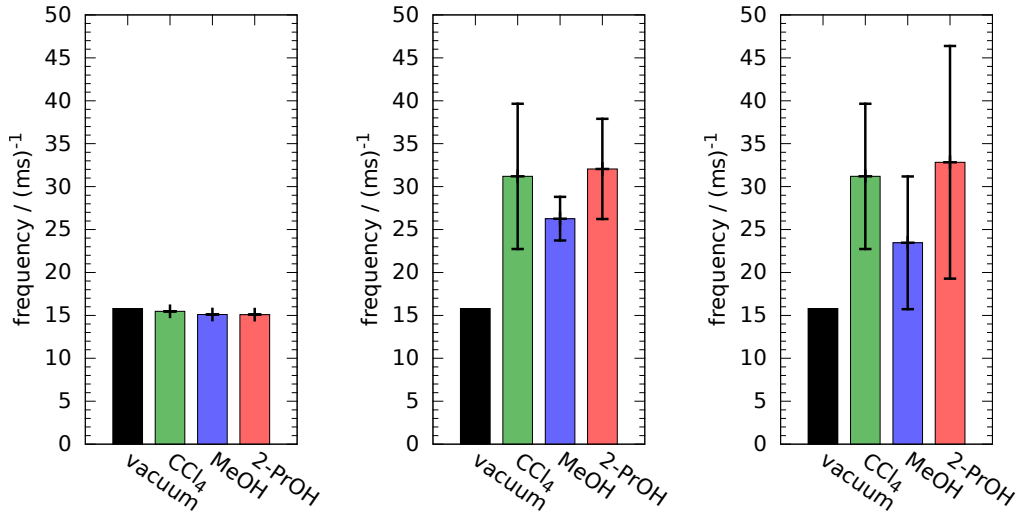

(a) $k0p0$ (b) $k0p1$ (c) $k2p2$

Figure 2: Averaged phosphorescence frequencies of 4*H*-pyran-4-thione obtained by the 2c-PERI-CCS method for different types of embedding potentials. The standard deviations are given in terms of error bars.